Focused on New Trends in Fatigue and Fracture

Visual Abstract

Characterisation and evaluation of the mechanical behaviour of endodontic-grade NiTi wires

Samuel Pereira
Instituto Superior Técnico, Universidade de Lisboa, Av. Rovisco Pais 1, 1049-001, Lisboa, Portugal
samuel.p.pereira@tecnico.ulisboa.pt

André Carvalho
CIMOSM - ISEL/IPL, Instituto Superior de Engenharia de Lisboa, Av. Conselheiro Emídio Navarro 1, 1959-007 Lisboa, Portugal
IDMEC – Instituto Superior Técnico, Universidade de Lisboa, Av. Rovisco Pais 1, 1049-001, Lisboa, Portugal
adcarvalho@dem.isel.pt

Luís Reis, Manuel Freitas
IDMEC – Instituto Superior Técnico, Universidade de Lisboa, Av. Rovisco Pais 1, 1049-001, Lisboa, Portugal
luis.g.reis@tecnico.ulisboa.pt, manuel.freitas@tecnico.ulisboa.pt

Diogo Montalvão
Department of Design and Engineering, Faculty of Science and Technology, Bournemouth University, Poole House, Talbot Campus, Fern Barrow, BH12 5BB, UK
dmontalvao@bournemouth.ac.uk

ABSTRACT. With the introduction of new materials and advances in medical science, the endodontic files have changed since the early days of root canal treatments. In the late days, we have seen an increasing use of Nickel-Titanium (NiTi) alloys. At body temperature, NiTi alloys present a superelastic behaviour, which allows to be more effective in the removal of the tooth pulp tissue, and in the protection of the tooth structure.
Anyhow, these NiTi instruments will eventually fracture, usually without any visual signal of degradation. Thus, there is a need of studying these alloys, as they present a high hysteresis cycle and non-linearities in the Elastic domain.
Currently, there is no international standard to test NiTi endodontic files, so various authors have attempted to design systems that can test them under fatigue loads, usually based on empirical setups.
Following a systematic approach, this work presents the results of rotary fatigue tests for two Alfa Aesar® Nitinol wires with different diameters (0.58mm and 0.25mm).The formulation is presented, where the material strength reduction can be quantified from the determination of the strain and the number of cycles until failure, as well numerical FEM simulation to verify the analytical model predictions.

OPEN ACCESS

Citation: Pereira, S., Carvalho, A., Reis, L., Freitas, M., Montalvão, D. Characterisation and Evaluation of the Mechanical Behaviour of Endodontic-grade NiTi Wires, Frattura ed Integrità Strutturale, 49 (2019) 450-462.

Received: 20.12.2018
Accepted: 10.05.2019
Published: 01.07.2019

KEYWORDS. Fatigue; Superelastic Alloys; NiTi wires; Life Evaluation

INTRODUCTION

Endodontic files have been used in dentistry since the middle ages and, as so, the shape, material and operation mode have changed since those days. These files are used in root canal procedures to remove the inflamed pulp and nerve endings in a tooth. In the past, endodontic files used in this procedure were made from highly flexible steel alloys. However, steel alloy files, while being flexible, are still too rigid to avoid damaging the walls of the root canals. [1-4] In order to minimise these adverse effects, Nickel-Titanium (NiTi) alloys are used in the design of endodontic files. This change in the material allowed the use of rotary systems to be used to prepare root canals more safely and predictably. [5] NiTi alloys are superelastic metal alloys able to fully recover from large deformations (up to strains of 10% [6]).

The Niti alloys, as others superelastic alloys, that are included in Shape Memory alloys family, present a particular behaviour for the stress vs strain plot, both on loading and unloading. On loading, the alloys start to present a linear phase, where the alloy presents a stable crystalline phase, known as austenite. After this first part, a second region of the plot shows a phase, also linear but with a much smaller slope and where occurs the transition from the austenitic phase to the martensitic phase. This transition phase is often referred as R-phase [7, 8], and a large strain is produced with a small variation of the stress. The third phase, in which the material presents a fully martensitic phase, is again linear and presents a greater slope than in the second region. During the unloading, the plot also presents three different parts, yet the stress plateau of the transition phase is much lower comparing to the loading. [9]

These alloys, however, have a drawback: when compared to steel files their fatigue life is relatively shorter than steel and, seen in commercial endodontic files, they break without a previous mechanical warning (such as visible plastic deformation), increasing the risk of the file failing inside the teeth. [10] To prevent these accidents the NiTi files are used only once, which leads to an increase of cost, making this material not that viable.

In order to increase the viability of the use of NiTi alloys in dentistry, some studies were made to determine the fatigue life of these alloys, usually through traditional uniaxial fatigue tests and rotary bending fatigue tests [11]. Although rotary bending tests are the tests that most accurately replicate the kind of loads and deformation a file is subjected to when inside a root canal, the great majority of the existing machines in the literature only perform the fatigue test with a predetermined set of shapes. However, most of the imposed deformations are far from the complex shapes of the root canals [12]. To work-around this problem, Cheung and Darvell in 2007 [12] and Carvalho et al. in 2015 [10] developed machines with a variable set shape, being able to evaluate the fatigue life of files and specimens in a more versatile way [13-16].

However, even with the efforts to characterise this material, the mechanical properties of NiTi change with the manufacturing process and, consequently, the mechanical behaviour during the endodontic procedure is highly variable. This variability creates the need to study NiTi alloys from different suppliers. In this work, the mechanical properties of Endodontic-grade NiTi wires, from Alfa Aesar®, will be studied both by experimental tests and numerical simulations. This paper is part of a research project that aimed to study the fatigue life of endodontic files. Since there is a plethora of different geometries and alloys (of which the manufactures do not disclose de composition), there is a need to compartmentalize the study. Studying a specimen with simple geometry, the results of the fatigue life can be directly correlated with the fatigue properties of the material itself. From this point forward, the study can be taken to the actual files, where the differences in fatigue life can then be corelated with the complex geometry of the files(the fatigue properties of the material are known).

For this, it is of special interest the rotary fatigue machine designed by Carvalho et al. (2015) [10], as this is the machine used to perform the fatigue test presented herewith. This machine consists of three pins that can be positioned precisely through numerical control to deform the test specimen with a degree of bending that can range from simple point bending to more complex multi-point bending, depending on the need of the user. The file/wire is then put into rotation using a brushless DC motor with variable speed, until failure is detected.

MATERIAL AND METHODOLOGY

Material

To perform the rotating fatigue four-point bending tests two NiTi alloy wires (Alfa Aesar® Nitinol wire) are used, with a composition of 55.75% Nickel and 44.25% Titanium. One with a diameter of 0.58mm and the other with a diameter of 0.25 mm, both straight annealed and with an oxide surface. [17]

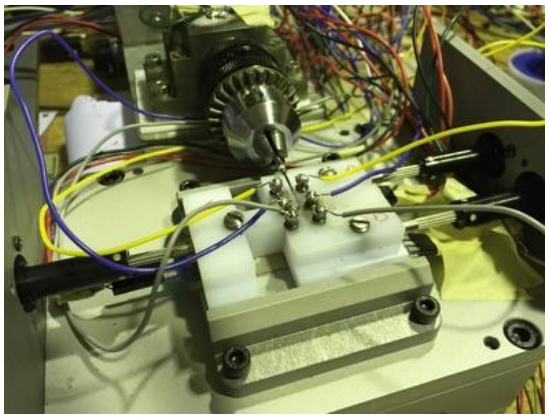

Figure 1: Test machine with an endodontic file [10].

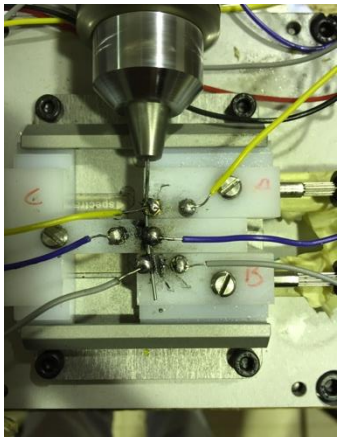

Figure 2: Test machine with the tree pins in a testing configuration [10].

Beam Model

To model the beam, one uses the Euler-Bernoulli beam theory, according to Eqn. (1)

$$EI\frac{d^4w}{dx^4}=q(x) \tag{1}$$

Where q(x) is the distributed transverse load, E is the Young's Modulus, I is the second moment of area of the cross section of the beam, x is the dimension across the length of the beam and w is the beam's deflection. Since there are no distributed transverse loads (only point loads due to the imposed displacement), (1) becomes:

$$\frac{d^4w}{dx^4}=0 \tag{2}$$

with the homogenous solution given by (3):

$$w(x)=C_1x^3+C_2x^2+C_3x+C_4 \tag{3}$$

Due to the discontinuous nature of the displacement application system, the beam must be divided into four sections, as seen in Fig. 3.

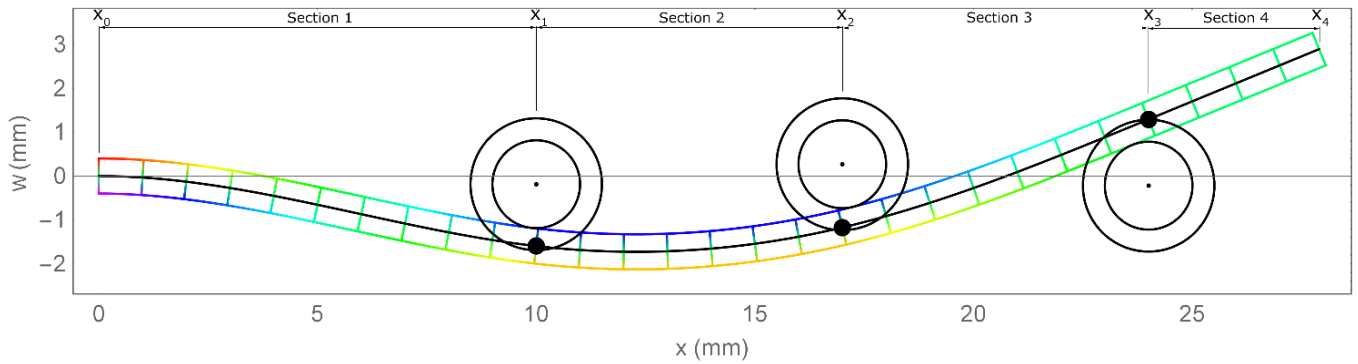

Figure 3: Beam model of the specimen, where x0 is the clamped end of the specimen; x1, x2 and x3 are the positioning pins; and x4 is the free end of the specimen [9]. Section 2 is the constant curvature section.

Using the boundary conditions (2), one can solve the equation for given pin displacements (W1, W2 and W3).

$$\begin{cases} w_1(x_0) = 0 \\ w_1'(x_0) = 0 \end{cases} \tag{2a}$$

$$\begin{cases} w_1(x_1) = w_2(x_1) = W1 \\ w_1'(x_1) = w_2'(x_1) \\ w_1''(x_1) = w_2''(x_1) \end{cases} \tag{2b}$$

$$\begin{cases} w_2(x_2) = w_3(x_2) = W2 \\ w_2'(x_2) = w_3'(x_2) \\ w_2''(x_2) = w_3''(x_2) \end{cases} \tag{2c}$$

$$\begin{cases} w_3(x_3) = w_4(x_3) = W3 \\ w_3'(x_3) = w_4'(x_3) \\ w_3''(x_3) = w_4''(x_3) \end{cases} \tag{2d}$$

$$\begin{cases} w_4''(x_4) = 0 \\ w_4'''(x_4) = 0 \end{cases} \tag{2e}$$

Knowing the shape of the deformed beam, the axial strain at any point can be determined by (3):

$$\varepsilon_x = -z\frac{d^2w}{dx^2} \tag{3}$$

where ε_x is the axial strain, and z is the radial coordinate of the point. If z is the radius of the wire, the resulting strain will be the surface strain (which has the highest absolute value, at each cross-section). With (3), one can reverse the computations and find what pin displacements are needed in order to obtain a constant strain in section 2, [10].
Instead of using the strain, one can also use the radius of curvature of the beam (ρ), which can be obtained by:

$$\frac{1}{\rho} = \frac{d^2w}{dx^2} \tag{4}$$

Uniaxial Tension Test

The uniaxial tension tests, with or without a hysteresis cycle, were performed with a nominal strain rate of $\dot{\varepsilon} = 0.1\,\text{min}^{-1}$ and the measurement on the extension, which later was converted to nominal strain, were obtained using a clip gauge. Only the wire of 0.58mm was used in this testing due to the slenderness of the thinner one with 0.25mm.
Besides the uniaxial tension test until rupture, the specimen was also subjected to one hysteresis cycle in order to determine their superelastic properties. The full hysteresis cycle can be obtained from loading the specimen in the elastic domain until the full transformation from Austenite into Martensite, and then reversing the process by unloading the specimen

Rotary Bending Test

The rotary fatigue bending tests were performed in the machine mentioned above and with a rotational speed of 500rpm (8.33 Hz). As it is a rotary fatigue test, the average stress is $\sigma_m = 0$ and the fatigue ratio is $R = \frac{\sigma_{min}}{\sigma_{max}} = -1$.

These tests were conducted up to 5% maximum strain for the 0.58mm wire and up to 3% for the 0.25mm wire, using the pin positions given by Tab. 1.

Strain	0.58mm wire				0.25mm wire			
	ρ (mm)	Pin 1 (mm)	Pin 2 (mm)	Pin 3 (mm)	ρ (mm)	Pin 1 (mm)	Pin 2 (mm)	Pin 3 (mm)
0.6%	48.3	-0.66	-0.479	0.516	20.83	-1.53	-1.097	1.155
0.8%	36.25	-0.88	-0.636	0.68	15.63	-2.03	-1.449	1.507
1%	29	-1.1	-0.792	0.84	12.5	-2.53	-1.794	1.846
2%	14.5	-2.19	-1.547	1.589	6.25	-5.02	-3.433	3.403
3%	9.67	-3.26	-2.266	2.271	4.17	-7.47	-4.973	4.843
4%	7.25	-4.33	-2.953	2.906	-	-	-	-
5%	5.8	-5.39	-3.615	3.512	-	-	-	-

Table 1: Pin positions and radius of curvature for the used strain levels.

Finite Element Analysis

A static structural Finite Element Analysis (FEA) was conducted in ANSYS 19.0 Workbench with the model shown in Fig. 4 to replicate the experiments conducted in the testing machine. The 0.58mm diameter wire was modelled with 10810 elements, and the 0.25mm diameter wire was modelled with 10850 elements, both with superelastic material properties showed in Tab. 1. The wire was clamped at one end and it was deformed under bending using three steel actuator pins that moved in the y direction based on the constant curvature formulation earlier presented. The movement of the actuators was simulated as being gradual, in an explicit iterative way. Contact properties were added between the actuator pins and the wire, with a considered frictional coefficient of 0.2, in order to mimic the experimental procedure [18].

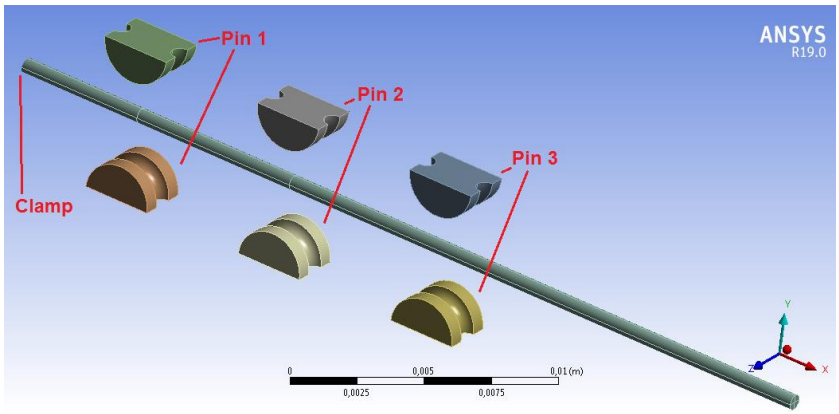

Figure 4: The FEA model with the clamp and the pins.

RESULTS FOR NITI WIRE

Uniaxial Tension and Uniaxial Fatigue Test

Before the rotary fatigue tests, the 0.58 specimen was tested under a uniaxial tension test and the results can be seen in Fig. 5, as well as the results, under the same conditions, for two other NiTi alloys [19].

Also, the specimen was subjected to one hysteresis cycle, Fig. 6, and the material properties obtained can be seen in Tab. 2.

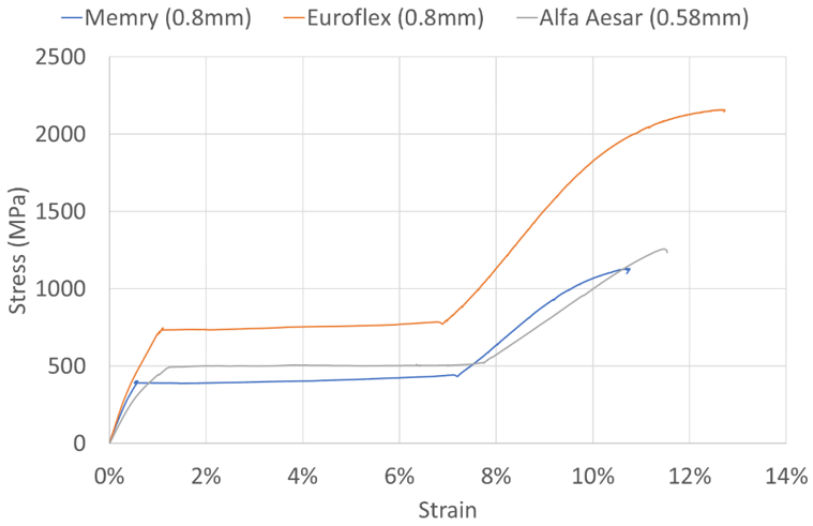

Figure 5: Uni-axial tension test results.

Material Property	Alfa Aesar®
Isotropic Elasticity	
Young's Modulus (GPa)	60
Poisson's Ratio	0.33
Superelasticity	
Starting stress value for the forward (Austenite to Martensite) phase transformation σ_s^{AS} (MPa)	522
Final stress value for the forward (Austenite to Martensite) phase transformation σ_f^{AS} (MPa)	555
Starting stress value for the reverse (Martensite to Austenite) phase transformation σ_s^{SA} (MPa)	280
Final stress value for the reverse (Martensite to Austenite) phase transformation σ_f^{SA} (MPa)	235
Maximum residual strains ϵ_L (mm/mm)	0.0645

Table 2: List of Material Properties to Alfa Aesar® Nitinol.

From Fig. 5, it can be seen that, while having the same overall behaviour with an elastic plateau (which is typical of NiTi alloys), there is a large variation in the ultimate tensile strength and phase transformation stress/strain necessary to start the phase transition, but not as such with regards to the overall strain and the "length" of the phase transformation region (i.e., the quasi-horizontal plateau).

Fatigue Tests

The results for the Strain vs Number of Cycles for the fatigue tests under different levels of strain induced in the 0.58mm and 0.25mm NiTi wires are presented in Fig. 7. In this figure it is also possible to see the fatigue results for two others different NiTi alloys tested in the same apparatus [19].

For the wire of 0.58mm diameter, the fatigue tests were conducted on a range of maximum extension from 0.6% to 5%. Where the specimens were subjected to strains under 1%, i.e., where the crystallography of the NiTi alloy still is austenitic, the material showed a large fatigue life, when compared with tests where specimens were subjected to larger levels of strain. More specifically, the 0.6% strain specimens, showed an infinite fatigue life (i.e., above 10^6 cycles).

The specimens with strains equal to and above 1% show a fatigue life nearly constant, in the order of magnitude of 10^2 to 10^3, as expected for superelastic alloys [20, 21]. The specimen with the shortest life time failed after 145 cycles.

For the specimens with 0.25mm diameter, the fatigue tests were conducted with a strain ranging from 0.6% to 3%. The specimens with strain under 1%, that correspond to the austenitic region, show a large fatigue life, when compared with the rest of points with some specimens showing an infinite fatigue life.
The specimens with strains equal to and above 1% show a decreasing fatigue life as the maximum imposed strain increases. The specimen with the shortest life time failed after 1989 cycles.

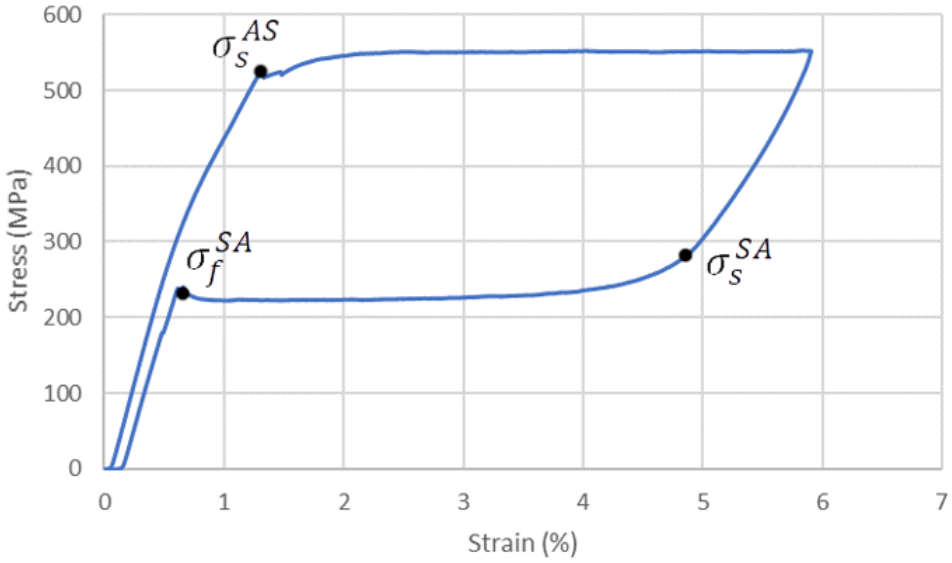

Figure 6: Uni-axial tension test with one hysteresis cycle, with the starting and final stress values for the forward and reverse transformations (the σ_f^{AS} is not reached in this test, because it marks the beginning of the plastic deformation regions).

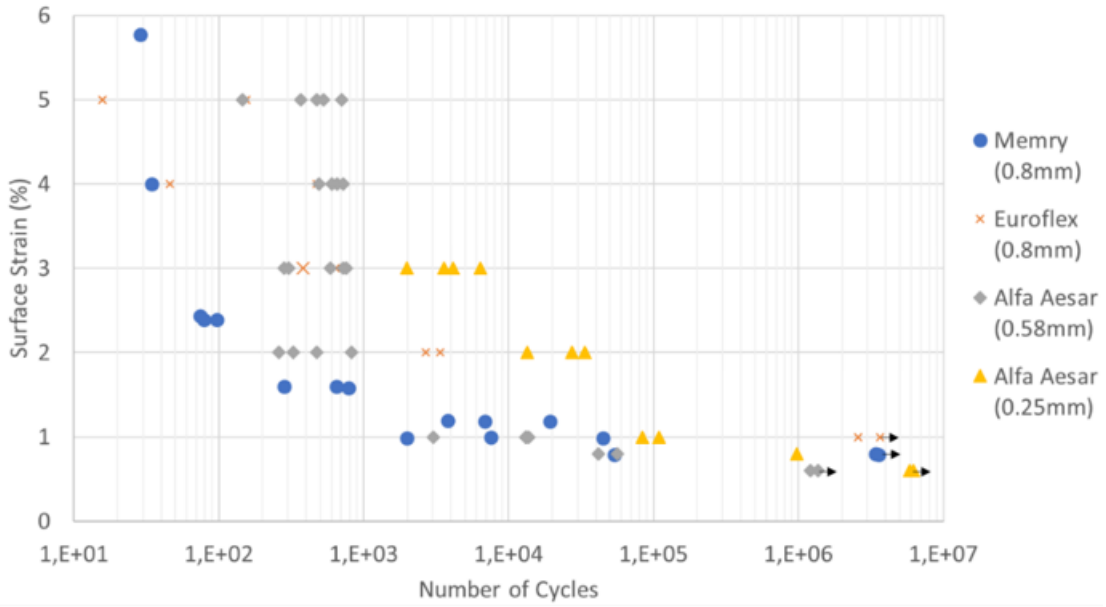

Figure 7: Surface Strain vs Number of Cycles. The surface strain is estimated using Eqn. (3).

It is also possible to see from Fig. 7 that all the alloys present an infinite life only when in austenitic phase, but not when under all strains during this phase. For a finite life time, the alloys tend to increase the life time with a decreasing diameter. This life time increase can be explained as a result of the energy absorption experienced by the material during the deformation. The energy per volume is given, for a uniaxial tension test, by the Eqn. (4) and, as the material is under the same strain, the energy absorption will increase with the volume.

$$\frac{energy}{volume} = \int_0^{\varepsilon_m} \sigma \, d\varepsilon \tag{4}$$

where ε_m is the maximum strain for the differential volume of material, and σ is the stress.
This behaviour is in line with the results found on the literature, as the NiTi alloys tend to increase the life time with a decreasing diameter. [22]

Fracture Surface

The fracture surfaces of the rotary bending tests were subjected to a closer look on a SEM (Scanning Electron Microscope). In Fig. 8, one can see that the surface shows some porosities that act like locations of stress concentrations where crack initiation can occur. This feature is not uncommon in other NiTi alloys but is not present in all of them. Also, after the rupture, the material presents a well-seen granular surface through which the fatigue fracture grew.

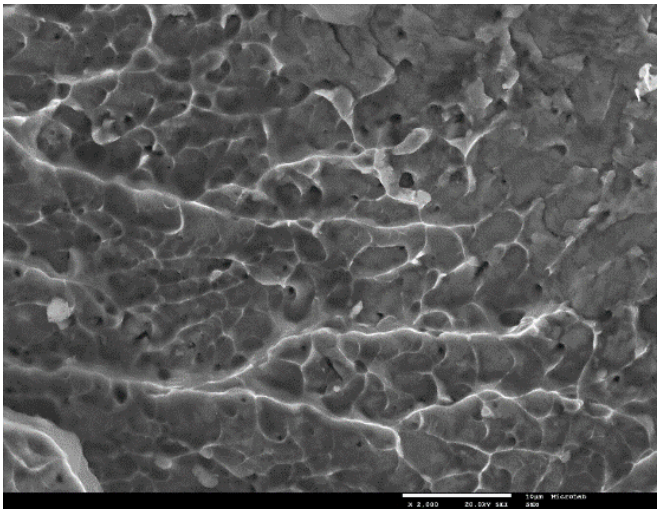

Figure 8: Detail of the porosities found in the alloy (2000x magnification).

The observation of the crack propagation zones showed, for the 0.58mm diameter wire, a similar size of crack propagation zone before the final rupture, for specimens obtained in the LCF zone, Fig. 9(a)-9(d). In Fig. 9(b), it can be seen a detail of a specimen tested under 5% of strain showing a small crack propagation zone near the surface. For lower strain (greater fatigue life time), the crack propagation zone size gets bigger as the strain levels decrease, resulting that the fracture propagates slower, Fig. 9(e). In Fig. 9(f), it can be seen a detail of a specimen tested under 1% of strain showing a greater crack propagation zone.
For the 0.25mm diameter wire, the analysis in the SEM showed that the crack propagation zone increases as the strain levels decrease. In Figs. 9(h) and 9(i) can be seen a detail of the crack initiation zone for a specimen tested under 2% of strain and 1% of strain, respectively, where this increase can be observed.

FEA Results - Normal stress

The results obtained for the normal stress on the x direction, between pin 1 and pin 2, for the different strain levels, are presented in Fig. 10, for both wires. The maximum compression stress (identified as Min, coloured in blue) occurs near the first actuator pin and is slightly greater than the maximum tension stress (identified as Max, coloured in red). The reason for this phenomenon is presumed to be the frictional contact friction between the pins and the wire, in order to mimic the real experiment.
The maximum stress randomly floats through the section 2, appearing near the first pin, but without a fixed location. Being a "constant strain region" according to the theoretical deformation model, the floating of the maximum tension stress location can only be attributed numerical error. Therefore, it is expected that the wires will fracture near the pin 1 due to friction

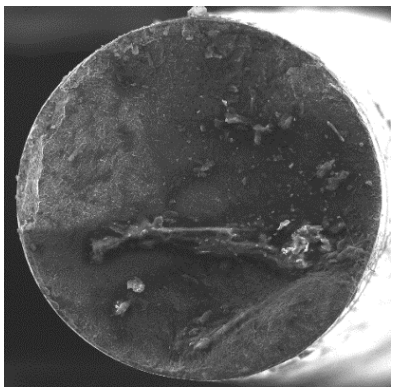

a: ε5% Ø0.58mm (x140

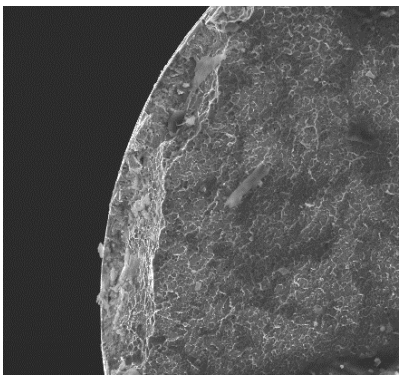

b: ε5% Ø0.58mm (x300 magnification)

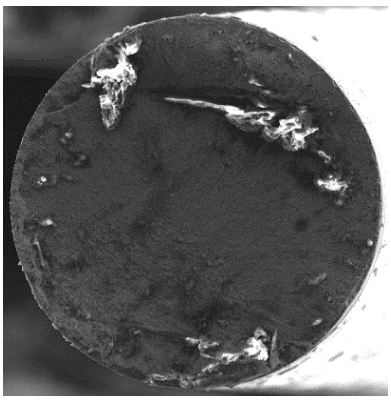

c: ε5% Ø0.58mm (x140 magnification)

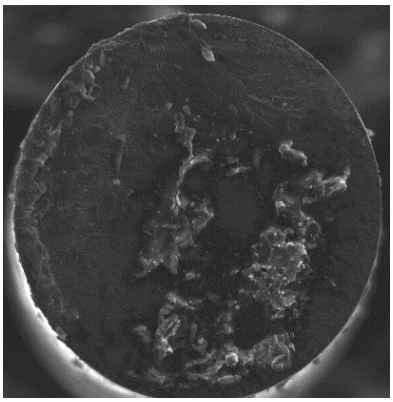

d: ε2% Ø0.58mm (x140

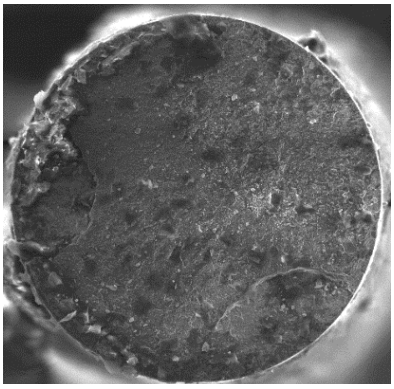

e: ε1% Ø0.58mm (x140 magnification)

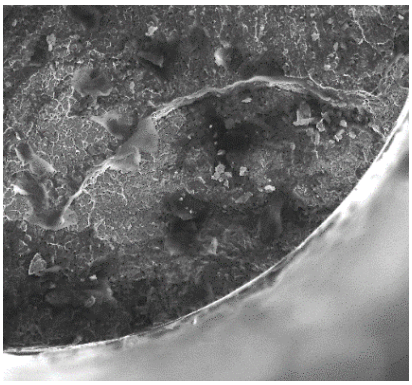

f: ε1% Ø0.58mm (x300 magnification)

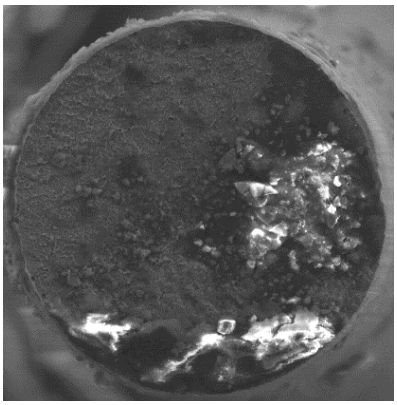

g: ε2% Ø0.25mm (x300 magnification)

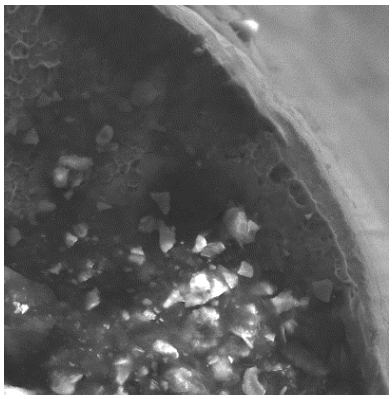

h: ε2% Ø0.25mm (x1000 magnification)

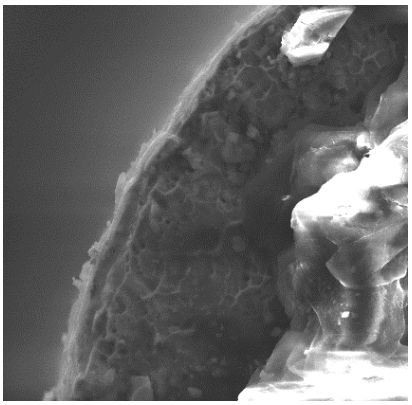

i: ε1% Ø0.25mm (x1000 magnification)

Figure 9: Fracture surfaces for several specimens.

The maximum value for the normal stress is being determined to be near the clamping region according to the FEA results. This should not be a surprise, because the clamping is modelled as being infinitely rigid. This leads to a stress concentration at this location, reason why the values can be quite significant. Since the true clamping region is very difficult to be modelled -accurately and the wires failed between the first two pins during the experiments, the analysis neglects the clamping location.

FEA Results - Normal Strain

The Finite Element model presents a maximum strain slightly lower than the theoretical Euler-Bernoulli beam model. For strains under and equal 1%, the relative error is small, but it increases with the deformation of the wire. This increase of error is among the expectations as the Euler-Bernoulli beam theory assumes the specimen to follow an isotropic elastic behaviour and small deformations, which happens for low strains than 1%; and does not provide accurate results to superelastic behaviour, which happens for greater strains.

In the charts of Fig. 11, can be seen the FEA strain vs the Maximum Theoretical Strain (MTS) for the 0.58mm diameter wire and the 0.25mm diameter wire, for both tension and compression, as the strain slightly differ.

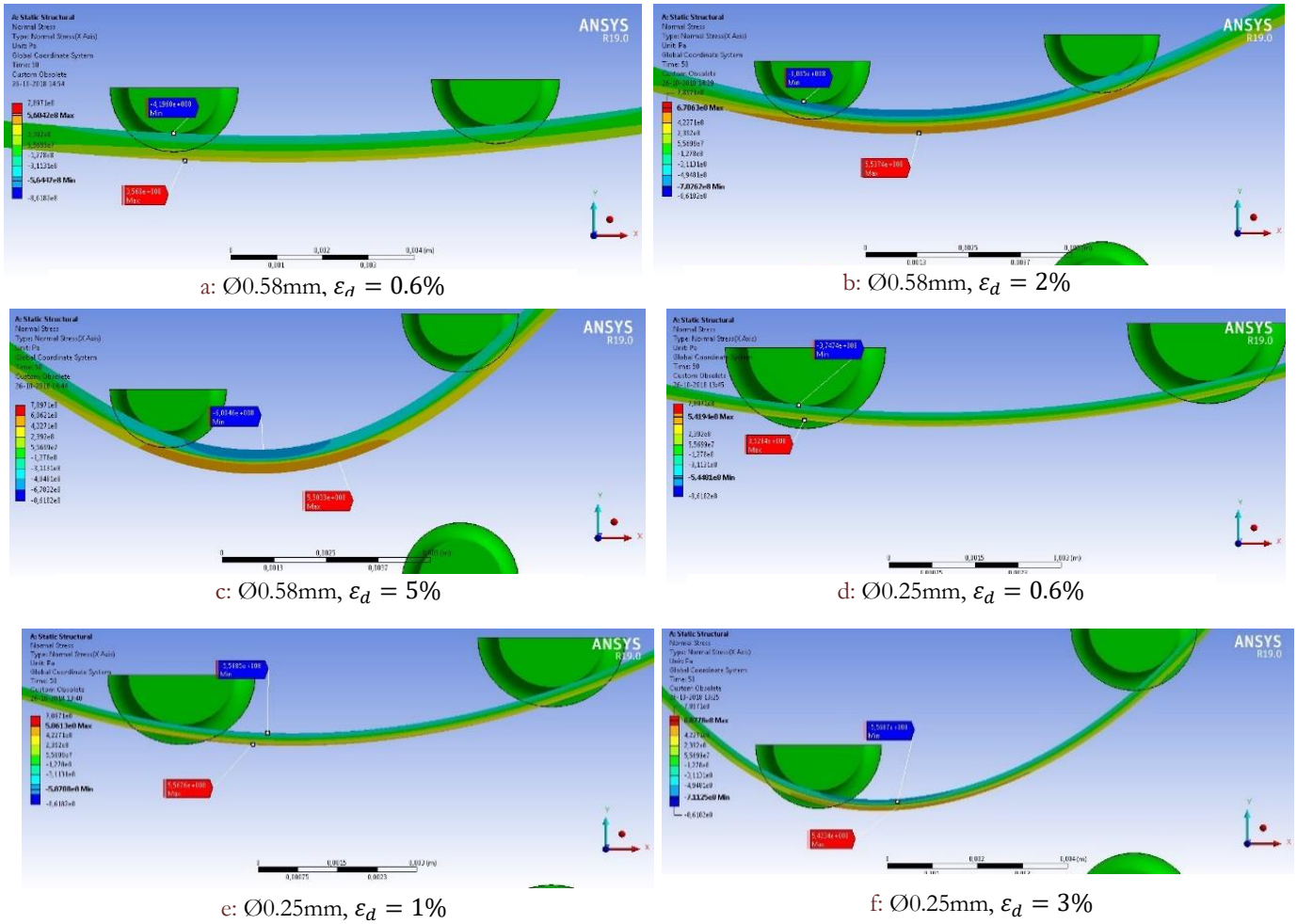

a: Ø0.58mm, $\varepsilon_d = 0.6\%$

b: Ø0.58mm, $\varepsilon_d = 2\%$

c: Ø0.58mm, $\varepsilon_d = 5\%$

d: Ø0.25mm, $\varepsilon_d = 0.6\%$

e: Ø0.25mm, $\varepsilon_d = 1\%$

f: Ø0.25mm, $\varepsilon_d = 3\%$

Figure 10: Stress distribution in the wires between pins 1 and 2

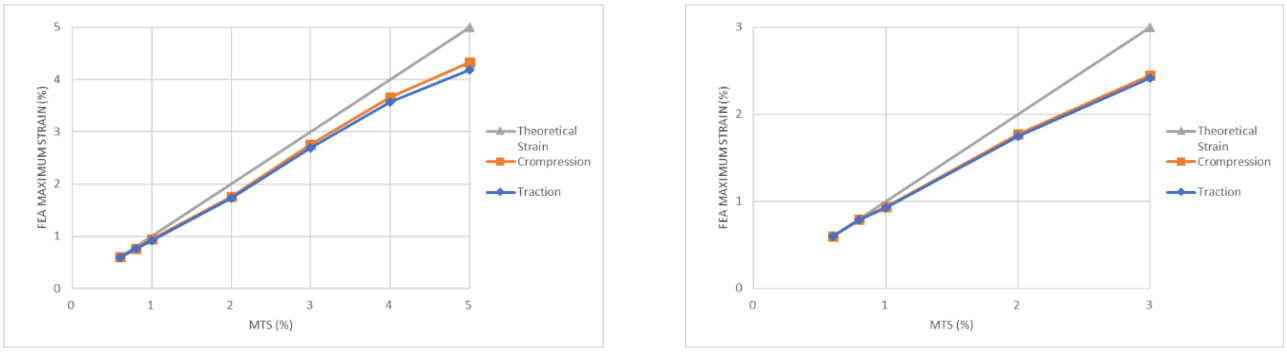

a: Ø0.58mm wire

b: Ø0.25mm wire

Figure 11: Comparison between Theoretical and FEA strains

FEA Results - Stress in the cross section of the Specimen

The stress along the cross section of the specimen shows the amount of material which is in the austenitic phase or already in the Austenite to Martensite transformation phase.

It can be seen in Fig. 12, for the region between pin 1 and pin 2, that some specimens, with low strain levels, show a linear change of stress along the cross section, suggesting that are still fully austenitic. In the other hand, the remaining specimens, under greater strain levels, show an inverted 'S' profile, meaning that they are partially austenitic (in the central zone, showing a straight line) and partially in the transformation phase (in the outer part, which is approximately flat) [6, 8, 23, 24].
Comparing the information obtained in these charts with the uniaxial tension results, the results converge as the 1% strain specimens present a fully austenitic cross section, as obtained in these tests. For strains above 1%, the wire starts to exhibit the transformation phase from Austenite to Martensite across the cross-section from the outer circle of the wire's cross-section towards its centre axis.

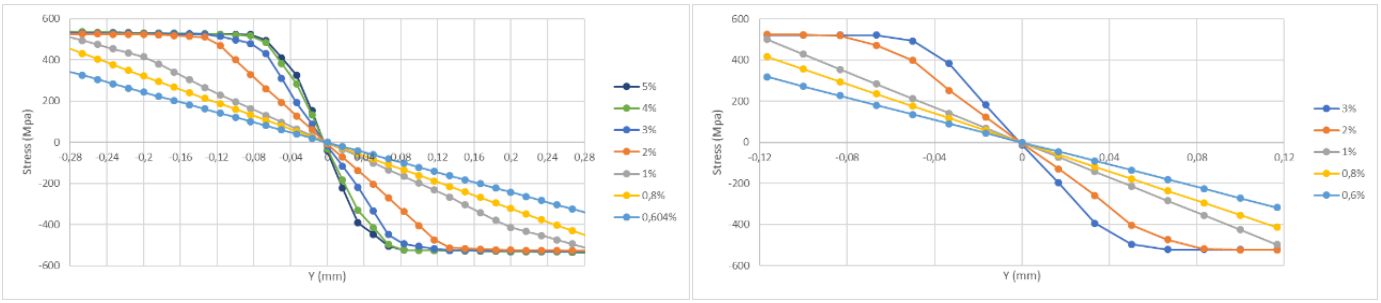

a: Ø0.58mm wire b: Ø0.25mm wire

Figure 12: Stress Profile along the beam cross section.

Final Results

After comparing the FEA results and the theoretical approach, as the results in terms of strain slightly differ, the combination of these two is imposed in order to improve the accuracy of the fatigue results presented.

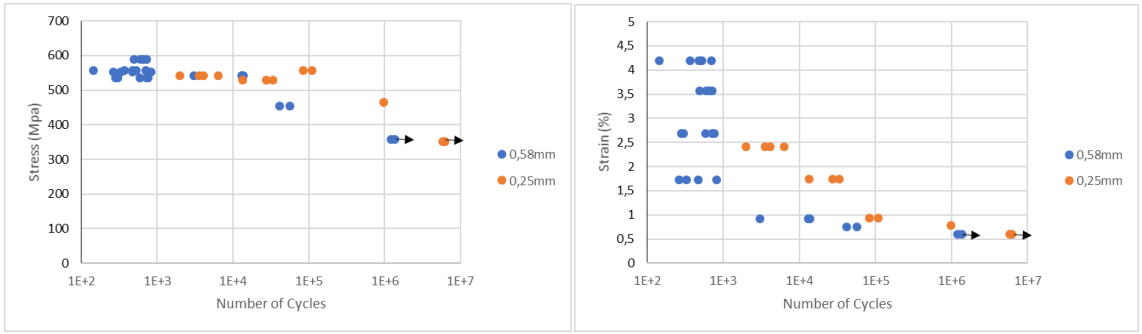

a – Stress vs Life Time b – Strain vs Life Time

Figure 13 - Stress vs Life Time concerning FEA and Laboratorial Results.

Conclusions and Future Work

The work developed and presented in this paper show the results obtained in the rotating bending machine developed by Carvalho et. al [10] and, later, the analysis and validation of both theoretical model and method used for that purpose.
The method used, as well as the machine used, allow to address a range of different issues and is able to analyse them based on sound Engineering foundations and Materials science. The versatility of the machine allows one to perform tests for different ranges of strains in a simple and intuitive way.
A series of fatigue tests were conducted using Alfa Aesar® Nitinol wires of two different diameters, one of 0.58mm and the other of 0.25mm diameter. The wires, when under strain levels in the elastic isotropic austenitic phase corresponding to strains of 0.6% and 0.8% for the 0.58mm and 0.25mm diameter wires, respectively, showed infinite (above 〚10〛^6 cycles) life time.
When under strain levels in the transformation phase condition, both wires showed a reduced fatigue life that is almost constant during this phase: between 145 and around 1000 cycles for the thicker wire with 0.58mm; and between 1989 and around 15000 cycles for the thinner wire with 0.25mm. This happens due to the stress-strain relation during this phase being

an almost constant plateau concerning to the stress. This is in line with the known behaviour of the NiTi alloys, in which the life time will be smaller than the one observed in this plateau only when it is tested under strains on the fully martensitic phase.

It can also be seen that, comparing the results of the two wires, the fatigue life of the thinner wire is always greater than the life time of the thicker one. This is in line with the literature, as for each different NiTi alloy, set of process parameters, and shape must be individually tested and analysed to provide accurate fatigue life data.

The analyses of the fracture surfaces allow to confirm the surfaces resulting from low cycle fatigue, showing a small crack propagation zone and a rough surface in the rest of the fracture surface, as the crack propagates fast and through the grain boundaries, as expected. As we move into the high cycle fatigue, the crack propagation zone increases, while the rest of the surface, where the crack propagates fast and through the grain boundaries, showed the same rough appearance.

Concerning the FEA, the results met the expectations and were validated from the theoretical model, showing an approximately constant strain zone between the first two pins. The specimens tend to present the highest value for the stress near the first pin, which statistically happened in the laboratory tests as that was the location where fracture occurred.

Still concerning the FEA, the stress across the beam showed that, as predicted, specimens up to 1% of strain are fully austenitic, while specimens with greater strain levels have the central part still in austenitic phase, while the outer part is already in the Austenite to Martensite transformation phase (R-Phase).

The comparison of FEA results with the theoretical model suggests that the models are suitable when the specimens are still in the isotropic elastic region. However, when the specimens start the Austenite to Martensite transformation, there is a slight loss in accuracy, although this is not significant to invalidate the FEA prediction of the fatigue life of the alloys tested.

For future work, other NiTi alloys used in endodontic files should be tested, as well as other alloys used in dentistry or other applications. Also, a greater range of rotary speeds should be tested to study the influence of this parameter in the fatigue life of these alloys. In order to improve the quality of the results, in special to improve the accuracy of the FEA, the thermal expansion coefficient of the materials studied should be considered, as well as the thermal energy dissipated during the rotary fatigue tests.

Acknowledgments

This work was supported by FCT, through IDMEC, under LAETA, project UID/EMS/50022/2019.

References

[1] Craig, R. G., McIlwain, E. D., and Peyton, F. A. (1968). Bending and torsion properties of endodontic instruments. Oral Surgery, Oral Medicine, Oral Pathology, 25(2), pp. 239–254. DOI: 10.1016/0030-4220(68)90286-7.

[2] Thompson, S. A. (2000). An overview of nickel-titanium alloys used in dentistry. International Endodontic Journal, 33(4), pp. 297–310. DOI: 10.1046/j.1365-2591.2000.00339.x.

[3] Civjan, S., Huget, E. F., and DeSimon, L. B. (1975). Potential Applications of Certain Nickel-Titanium (Nitinol) Alloys. Journal of Dental Research, 54(1), pp. 89–96. DOI:10.1177/00220345750540014301.

[4] Schafer, E. (2002) Metallurgie und Eigenschaften von Nickel-Titan-Instrumenten zur maschinellen Wurzelkanalaufbereitung. In: Hulsmann, M., editor. Wurzelkanalaufbereitung mit Nickel-Titan-Instrumenten. Ein Handbuch. Berlin: Quintessenz, pp. 35–46

[5] Krupp, D., Brantley, J., and Gerstein, H. (1984). An investigation of the torsional and bending properties of seven brands of endodontic files. Journal of Endodontics, 10(8), pp. 372–380. DOI: 10.1016/s0099-2399(84)80157-0.

[6] Montalvão, D., Alçada, F. S., Braz Fernandes, F. M., and de Vilaverde-Correia, S. (2014). Structural Characterisation and Mechanical FE Analysis of Conventional and M-Wire Ni-Ti Alloys Used in Endodontic Rotary Instruments. The Scientific World Journal, pp. 1–8. DOI: 10.1155/2014/976459.

[7] Nagasawa, A., (1970). A new phase transformation in the NiTi alloy. Journal of the Physical Society of Japan, 29(5), pp.1386-1386.

[8] Ling, H. C., and Kaplow, R. (1981). Macroscopic length changes during the B2 ⇆ R and M → B2 transitions in equiatomic Ni-Ti alloys. Materials Science and Engineering, 51(2), pp. 193–201. DOI: 10.1016/0025-5416(81)90195-6.

[9] Montalvão, D., Shengwen, Q., and Freitas, M. (2014). A study on the influence of Ni–Ti M-Wire in the flexural fatigue life of endodontic rotary files by using Finite Element Analysis. Materials Science and Engineering: C, 40, pp. 172–179. DOI: 10.1016/j.msec.2014.03.061.
[10] Carvalho, A., Freitas, M., Reis, L., Montalvão, D., and Fonte, M. (2015). Rotary Fatigue Testing Machine to Determine the Fatigue Life of NiTi alloy Wires and Endondontic Files. Procedia Engineering, 114, pp. 500–505. DOI: 10.1016/j.proeng.2015.08.098.
[11] Plotino, G., Grande, N. M., Cordaro, M., Testarelli, L., and Gambarini, G. (2009). A Review of Cyclic Fatigue Testing of Nickel-Titanium Rotary Instruments. Journal of Endodontics, 35(11), pp. 1469–1476. DOI: 10.1016/j.joen.2009.06.015.
[12] Cheung, G. S. P., and Darvell, B. W. (2007). Fatigue testing of a NiTi rotary instrument. Part 1: strain-life relationship. International Endodontic Journal, 40(8), pp. 612–618. DOI: 10.1111/j.1365-2591.2007.01262.x.
[13] Plotino, G., Grande, N. M., Melo, M. C., Bahia, M. G., Testarelli, L., and Gambarini, G. (2010). Cyclic fatigue of NiTi rotary instruments in a simulated apical abrupt curvature. International Endodontic Journal, 43(3), pp. 226–230. DOI: 10.1111/j.1365-2591.2009.01668.x.
[14] Lopes, H. P., Britto, I. M. O., Elias, C. N., Machado de Oliveira, J. C., Neves, M. A. S., Moreira, E. J. L., and Siqueira, J. F. (2010). Cyclic fatigue resistance of ProTaper Universal instruments when subjected to static and dynamic tests. Oral Surgery, Oral Medicine, Oral Pathology, Oral Radiology, and Endodontology, 110(3), pp. 401–404. DOI: 10.1016/j.tripleo.2010.05.013.
[15] Gambarini, G., Gergi, R., Naaman, A., Osta, N., and Al Sudani, D. (2012). Cyclic fatigue analysis of twisted file rotary NiTi instruments used in reciprocating motion. International Endodontic Journal, 45(9), pp. 802–806. DOI: 10.1111/j.1365-2591.2012.02036.x
[16] De-Deus, G., Moreira, E. J. L., Lopes, H. P., and Elias, C. N. (2010). Extended cyclic fatigue life of F2 ProTaper instruments used in reciprocating movement. International Endodontic Journal, 43(12), 1063–1068. DOI: 10.1111/j.1365-2591.2010.01756.x
[17] Alfa Aesar by Thermo Fisher Scientific (2018) https://www.alfa.com/pt/nitinol-nickel-titanium-shape-memory-alloys/
[18] Zhao, H., Liu, L., Hu, W., and Shen, B. (2007). Friction and wear behavior of Ni-graphite composites prepared by electroforming. Materials and design, 28(4), pp. 1374-1378. DOI: 10.1016/j.matdes.2006.01.001.
[19] Carvalho, A., Freitas, M., Reis, L., Montalvão, D., and Fonte, M. (2016). Rotary Fatigue Testing to Determine the Fatigue Life of NiTi alloy Wires: An Experimental and Numerical Analisys. Procedia Structural Integrity, 1, pp. 34–41. DOI: 10.1016/j.prostr.2016.02.006.
[20] Ueland, S. M., and Schuh, C. A. (2012). Superelasticity and fatigue in oligocrystalline shape memory alloy microwires. Acta Materialia, 60(1), pp. 282–292. DOI: 10.1016/j.actamat.2011.09.054.
[21] Mahtabi, M. J., Shamsaei, N., and Mitchell, M. R. (2015). Fatigue of Nitinol: The state-of-the-art and ongoing challenges. Journal of the Mechanical Behavior of Biomedical Materials, 50, pp. 228–254. DOI: 10.1016/j.jmbbm.2015.06.010.
[22] Norwich, D. W., and Fasching, A. (2009). A Study of the Effect of Diameter on the Fatigue Properties of NiTi Wire. Journal of Materials Engineering and Performance, 18(5-6), pp. 558–562. DOI:10.1007/s11665-009-9415-9.
[23] Nagasawa, A. (1970). A New Phase Transformation in the NiTi Alloy. Journal of the Physical Society of Japan, 29(5), pp. 1386–1386. DOI: 10.1143/jpsj.29.1386.
[24] Paula, A. S., Mahesh, K. K., dos Santos, C. M. L., Canejo, J. P. H. G., and Fernandes, F. M. (2006). One-and two-step phase transformation in Ti-rich NiTi shape memory alloy. International Journal of Applied Electromagnetics and Mechanics, 23(1, 2), pp. 25-32.